Advanced Composite Materials
Publication details, including instructions for authors and subscription information:
http://www.tandfonline.com/loi/tacm20

Effect of IFSS on tensile strength of unidirectional fiber composites using 3D-FEM simulation

Koichi Goda , Yoshikazu Miwa & Hitoshi Kodama
Version of record first published: 02 Apr 2012.

To cite this article: Koichi Goda , Yoshikazu Miwa & Hitoshi Kodama (2003): Effect of IFSS on tensile strength of unidirectional fiber composites using 3D-FEM simulation , Advanced Composite Materials, 12:1, 73-89

To link to this article: http://dx.doi.org/10.1163/156855103322320383

Adv. Composite Mater., Vol. 12, No. 1, pp. 73–89 (2003)

Also available online - www.vsppub.com

Effect of IFSS on tensile strength of unidirectional fiber composites using 3D-FEM simulation

KOICHI GODA [1,*], YOSHIKAZU MIWA [2] and HITOSHI KODAMA [3]

[1] *Department of Mechanical Engineering, Yamaguchi University, Ube, Japan*
[2] *Graduate School of Science and Engineering, Yamaguchi University, Ube, Japan*
[3] *ACM Technology Department, Mitsubishi Rayon Co., Ltd., Tokyo, Japan*

Received 9 January 2003; accepted 15 April 2003

Abstract—A Monte-Carlo simulation model based on 3D-finite element analysis was developed to clarify the effect of interfacial shear strength (IFSS) on tensile strength of a unidirectional composite with fibers placed in a hexagonal array. The simulation model comprises fiber, matrix and interface elements; thereby, fiber breaks, matrix fractures and interfacial debondings during loading can be predicted individually. Tensile fracture processes and strengths of a boron/epoxy composite were simulated at various IFSSs. Results show that as IFSS decreases, stress concentration factors to intact fibers adjacent to a broken fiber element decrease because of occurrences of interfacial debonding. However, since interfacial debonding also reduces load carrying capacity in broken fibers, composite strength is reduced in all fiber volume fractions. On the other hand, a large IFSS causes many matrix fractures at once; therefore, it induces low composite strength. Thus, intermediate IFSSs increase tensile strength of the composite. This means that there must be an 'optimum' IFSS which induces the highest tensile strength of the composite. The optimum value shifts to a low value as fiber volume fraction increases. This occurs because the matrix around broken fiber elements becomes more apt to be broken easily in shear at a higher fiber volume fraction, therefore enhancing normal stress on intact fibers.

Keywords: Unidirectional composites; tensile strength; interfacial shear strength; interfacial debonding; finite element method; Monte-Carlo simulation; Weibull distribution.

1. INTRODUCTION

Advanced composite materials reinforced with continuous fibers, such as carbon, aramid and boron, are increasingly applied in structural materials requiring high reliability and durability. Since such composites are composed of different constituents, their fracture behaviors involve a complicated damage accumulation

*To whom correspondence should be addressed. E-mail: goda@po.cc.yamaguchi-uac.jp

process resulting from random fiber breakage, stress transfer from broken to intact fibers, and debonding between the fiber and matrix. The Monte-Carlo simulation technique coupled with a stress analysis method is one of the most effective tools for understanding this process. For example, the shear-lag model [1] has been used in many studies as a stress analysis method for predicting composite microdamage [2–5]; it has been applied for developing Monte-Carlo simulation techniques [6–10]. The finite element method (FEM) is also an effective stress analytical method, especially in expressing simultaneously the effects of tension and shear on the matrix, and its elasto-plastic time-dependent deformation [11]. Furthermore, FEM can simulate interfacial debonding by placing a double-node at the interface between the fiber and matrix, apart from simulating matrix fractures [12]. On the other hand, several theoretical models for statistically predicting composite strength have also been proposed. However, local and global load-sharing rules [13] used in the models are quite limited in their ability to precisely model the effects of interfacial bond properties and matrix mechanical properties on composite strength.

It is widely known that interfacial strength between the fiber and matrix can significantly influence axial tensile strength of unidirectional fiber composites [14, 15]. That is, low interfacial bond strength promotes large-scale debonding around broken fibers and reduces their load-carrying capacity. On the other hand, high interfacial bond strength tends to extend cracks transversely into the matrix at fiber breaks; this extension results in increasing stress concentrations to intact fibers around these breaks. The same phenomenon occurs when matrices are brittle. Such large-scale debonding and matrix-cracking are major factors in reducing strength of polymer [16, 17] and metal [9] matrix composites. Therefore, one of the authors developed a FEM simulation model to clarify the effect of interfacial shear strength (hereinafter, referred to as 'IFSS') on the tensile strength of a planar composite [12]; he inferred that there must be an optimum IFSS which increases tensile strength. Such a possibility may also occur in the structure of a real composite, such as a composite with fibers placed in hexagonal geometry. Thus, this paper is intended to develop a 3D-FEM simulation model and predict effects of IFSS on tensile strength of the hexagonally-placed fiber composite.

2. ANALYTICAL METHOD

2.1. Finite element model and mesh

Figure 1 shows the model and mesh of the present simulation; a 2-node line element representing a fiber element is incorporated into nodes along the z-axis of a 6-node triangular prism element representing a matrix element. The fiber element is a linear elastic body with random breaks; the matrix element is also an elastic body, which can simulate a multi-axial stress state caused by both tensile and shear stresses around fiber break(s). On the other hand, spring elements are often used for treating problems of delamination between plies [18] and interfacial cracks [19].

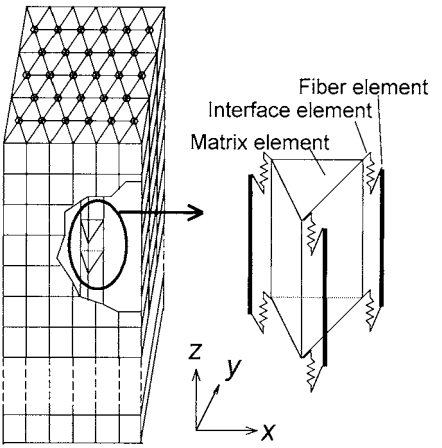

Figure 1. Finite element model and mesh.

Thus, in this study, a shear spring element is applied for expressing resistance for interfacial shear debonding. This element represents an interface bonding layer (referred to as the 'interface element') and connects the fiber and matrix elements at their nodes, as shown in Fig. 1. Then, a stiffness matrix of the shear spring element is determined by the size and shear modulus of the interface bonding layer, similar to formulation of a 2-node line element. A global stiffness matrix is constituted from stiffness matrices of these three kinds of elements; therefore, the entire structural analysis can be carried out based on an ordinary finite element method. Epoxy matrix used here is a relatively brittle material including a small scale of plastic deformation. Therefore, as mentioned above, the constitutive equation of this matrix material is assumed as an elastic body for simplicity. This assumption means a sufficient condition such that unidirectional composites indicate a peak in strength with increasing IFSS, because this peak appears more obviously if the matrix exhibits a smaller fracture energy [9].

Each element is statically fractured when the stress acting on the element satisfies a fracture criterion. Fractures of these elements were treated in the simulation as follows: The Young's modulus of a fiber element is changed to zero if its normal stress achieves a tensile strength which is assigned from a Weibull random number. The shear modulus of an interface element is changed to zero if its shear stress achieves an IFSS. The von Mises criterion is applied for the fracture of a matrix element. That is to say, the Young's modulus of a matrix element is changed to zero when the equivalent stress of this element achieves its tensile strength. Hereafter, we often denote each fracture as 'damage'; individually, those of fiber, matrix and interface elements are called 'fiber breaks', 'matrix fractures' and 'interfacial debondings', respectively.

Material simulated herein is a boron/epoxy composite with twenty-three fibers placed in a hexagonal array, as numbered in Fig. 2. (The composite is shown as a rectangular prism in Fig. 1, but side elements are removed for actual computation,

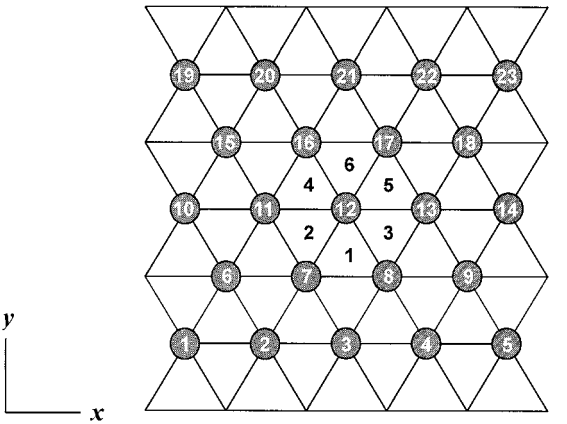

Figure 2. Numbered fibers and matrices in $x-y$ plane.

as shown in Fig. 2.) The matrix is also numbered for six regions at the center in the $x-y$ plane, as shown in Fig. 2. Each of these constituents is divided into 25 elements along the z-axis. Consequently, the number of nodes is 1612, the number of fiber, matrix and interface elements are 575, 1350 and 552, respectively.

2.2. Simulation procedure

Occurrences of fiber breaks, matrix fracture and interfacial debonding would cause a complicated stress distribution throughout a composite. Therefore, a method for estimating reasonably what type of damage occurs on each element should be incorporated into the simulation procedure. This study employs the $r_{\min}$ method to calculate this estimation exactly [11, 12]; it has been used to clarify yielding regions in a metal by means of an elastic–plastic finite element method. According to this method, a ratio of the difference between strength and stress on each element to a stress increment, r, is calculated for all elements. Only an element giving the minimum ratio, $r_{\min}$, takes precedence for fiber break, matrix fracture or interfacial debonding. The simulation procedure is as follows.

(1) Fiber strength obeys the following 2-parameter Weibull distribution:

$$F(\sigma) = 1 - \exp\left\{-\frac{L}{L_0}\left(\frac{\sigma}{\sigma_0}\right)^m\right\}, \tag{1}$$

where m and σ_0 are the Weibull shape and scale parameters, L is an arbitrary fiber length, which in this study is equivalent to the fiber element length, L_0 is a standard gage length at which the Weibull parameters were estimated. By substituting a uniform random number into the inverse function of equation (1), we can generate a random Weibull strength assigned to a fiber element.

(2) Unknown nodal displacement increments are first computed under the boundary condition of displacement increments applied at the ends of the fibers and matrix. A composite stress is then calculated by dividing support forces at the

ends along the z-axis by the cross-sectional area of the composite. Computation is carried out incrementally, but numerical values of the boundary condition are not fixed. That is, a temporary displacement increment ΔZ^*, sufficient to damage almost all elements, is given to the ends even at the first calculation stage; also, temporary stresses and stress components acting on the elements are calculated from computed displacement increments. Additionally, ratios r of all elements are calculated.

(3) Next, the element presenting the highest possibility of damage occurrence is determined from the minimum of the ratios, $r_{\min}$, as follows:

(i) If $r_{\min} \leqslant 1$, then all temporary displacement increments calculated at this stage are corrected to exact displacement ones by multiplying $r_{\min}$ by each temporary displacement increment as shown in Fig. 3a. In this stage, [D] matrix components on an element giving the $r_{\min}$ are also changed to zero. If this element is a fiber element or a matrix element, then in the next stage, as shown in Fig. 3b, the load acting on this element is released through its nodes along the z-axis under the boundary condition of load increment and the fixed condition at the fiber and matrix ends. If '$r_{\min} \leqslant 1$' is

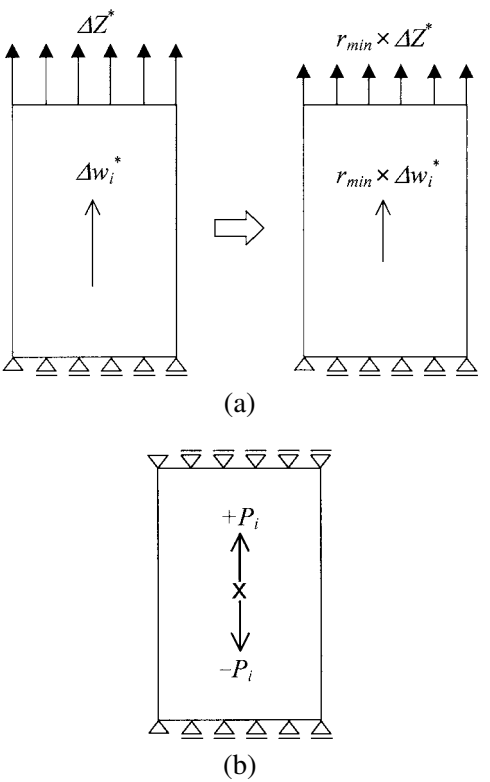

Figure 3. Calculation methods (a) for correction of displacement increments Δw_i^* using the $r_{\min}$ method, and (b) for releasing a fracture load.

still satisfied, the next stage is enacted to release the load acting on a new damaged element in the same way, together with the residual load(s) at the previous stage. This procedure is repeated until $r_{\min} > 1$.

(ii) If $r_{\min} > 1$, no damage occurs. Then, the boundary condition of displacement increments is applied again at the ends of fibers and matrix, as described in (2).

(4) As damage accumulates in a composite, support forces at the ends begin to decrease largely at a certain strain level. It was assumed that the composite's fracture criterion is satisfied when composite stress achieves a stress level less than 80% of the maximum composite stress. The maximum composite stress corresponds to a tensile strength, which is obtained in one simulation. The simulation was repeated five to six times for each condition using different Weibull random numbers. Results shown later in figures are averages of simulated strengths.

2.3. Material constants

This study simulates tensile strength of a boron/epoxy composite. Material constants are as follows:

$$D_f = 0.142 \text{ mm}, \quad E_f = 397.9 \text{ GPa}, \quad E_m = 3.30 \text{ GPa}, \quad \nu_m = 0.39,$$
$$\sigma_m = 45.6 \text{ MPa}, \quad G_i = 1.19 \text{ GPa},$$
$$t_i = D_f/100, \quad \Delta l = 0.716 \text{ mm}, \quad m = 7.16, \quad \sigma_0 = 3.665 \text{ GPa},$$

where D_f is the fiber diameter, E_f is the Young's modulus of the fiber, E_m is the Young's modulus of the matrix, ν_m is the Poisson ratio of the matrix, σ_m is the tensile strength of the matrix, G_i is the shear modulus of the interface bonding layer. Also, t_i is the thickness of the interface bonding layer, which was assumed as a small quantity (1/100) in this simulation because an interface bonding layer is actually negligibly thin and is employed as a model to express an interfacial debonding. However, the thickness value can be determined by matching optically measured and calculated interfacial debonding lengths in a planar composite plate [12]. Δl is the length of an element along the z-axis. The reinforcing fiber is a boron fiber, which has a diameter of 142 μm (5.6 mil) produced by AVCO; the matrix is an epoxy resin supplied by Ciba-Geigy Co. (Arardite CY230/Hardner HY2967). Weibull parameters for boron fiber strength, Young's modulus, and tensile strength of the epoxy were obtained by experiment [12]. The shear modulus of the interface element was assumed to be equal to that of the epoxy. It is also assumed that interface element widths correspond to the fiber circumference. In the present model, fiber spacings of 0.358, 0.179, 0.119, and 0.0895 were given, which correspond to fiber volume fractions V_f, of 0.108, 0.327, 0.522, and 0.660, respectively.

3. RESULTS AND DISCUSSION

3.1. Fiber stress distribution

Stress distributions of fiber elements were calculated at $V_f = 0.108, 0.327, 0.522,$ and 0.660 using the present FEM simulation model on the condition that the element located at the center of fiber 12 was intentionally broken at the fiber stress of 2500 MPa. Figures 4a and 4b show stress distributions of fibers 11 (or 7, 8, 13, 16, 17) and 12, in which stresses are normalized by dividing them by an average of all fiber stresses. To compare normalized stress with analytical stress concentration factors, it is assumed in this calculation that no interfacial debonding or matrix fracture occurred in the composite. Results show that fiber stress distributions are almost identical for any fiber volume fraction. As shown in the Fig. 4a, fiber breakage induces stress enhancement to the intact fiber 11. The enhanced stress of fiber 11 is approximately equivalent to a stress concentration factor (hereinafter referred to as 'SCF'). Table 1 lists SCF for each fiber volume fraction. The SCF increases slightly as fiber volume fraction increases. These SCF values are slightly

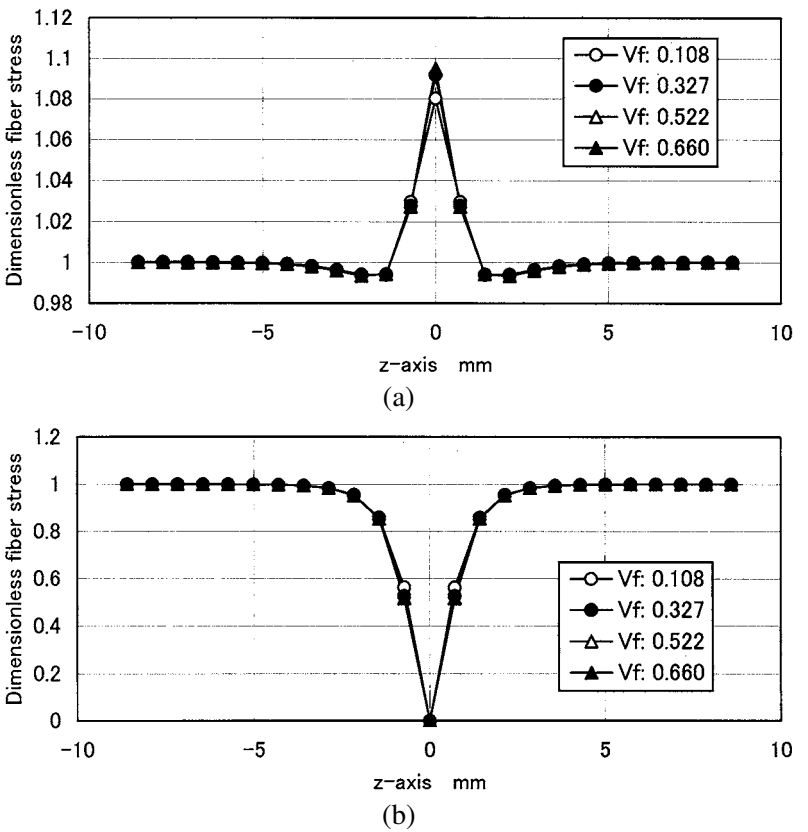

Figure 4. Normalized stress distributions of intact and broken fibers at a high IFSS. (a) Fiber 11. (b) Fiber 12.

Table 1.
Stress concentration factors (SCFs) to intact fibers adjacent to broken fiber 12

Fiber volume fraction	0.108	0.327	0.522	0.660
SCF	1.080	1.092	1.094	1.095
SCF including matrix stress	1.102	1.098	1.097	1.097
SCF (Hedgepeth and Dyke)		1.104		
SCF (Suemasu)		1.105		

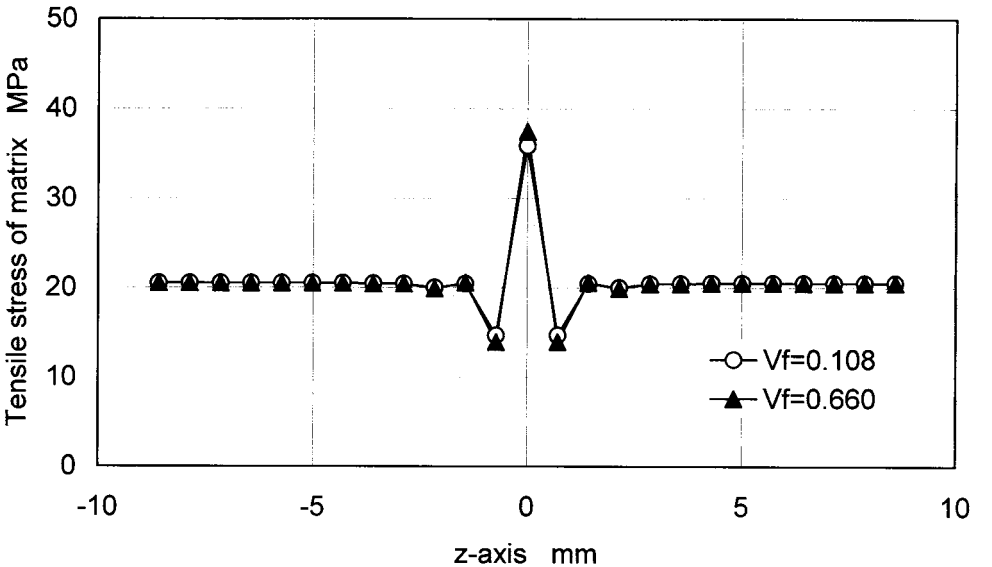

Figure 5. Tensile stress distribution along z-axis of matrices 1 and 6 adjacent to broken fiber 12.

less than SCFs analyzed from shear-lag models by Hedgepeth and van Dyke [20] and Suemasu [21], i.e. 1.104 and 1.105, respectively. Figure 5 shows normal stress distributions of matrices 1 and 6 along the z-axis at $V_f = 0.108$ and 0.660. As seen in the figure, stress distributions are almost equal, independent of fiber volume fraction. Also, it should be noted that stress enhancement also occurs at the matrix element adjacent to the broken fiber element. We found from calculation that this stress enhancement is imposed mainly on six matrices, 1, 2, 3, 4, 5, and 6, adjacent to broken fiber 12. That is to say, the load transferred from the breakage is imposed not only on intact fiber elements, but also on adjacent matrix elements. We also found that each of the six matrix elements sustained extra normalized stresses of 2.2×10^{-2}, 5.6×10^{-3}, 2.6×10^{-3} and 1.5×10^{-3} at $V_f = 0.108$, 0.327, 0.522 and 0.660, respectively. By adding these extra values to SCFs, they were modified as shown in Table 1. Modified SCFs are not changed so drastically, but are comparable to SCFs of Hedgepeth and van Dyke, and Suemasu. This result also indicates that, although the finite element mesh used here is relatively coarse, calculated SCFs are approximately equal to shear-lag solutions.

3.2. Fiber stress distribution with interfacial debonding

Stress enhancement occurs not only on intact fibers adjacent to the broken fiber element, but also on another located sixteen intact fibers away from the broken one. Figure 6a shows SCFs to all intact fibers in the same plane of broken fiber element at conditions of $V_f = 0.327$ and IFSS = 73.5 MPa, in which no interfacial debonding or matrix fracture were included. It is seen that SCF is less when location of intact fibers is farther away from the broken fiber element. In this case, the sum of all SCFs was 22.96, which is slightly less than 23, the total number of fibers. As implied in the above, its balance, 0.04 (= 23 − 22.96), is sustained by the matrix. Figures 6b and 6c show SCFs at IFSS = 39.2 MPa and 19.6 MPa. Calculations were also carried out in the same condition as the above. As shown in the figures, SCFs to intact fibers 7, 8, 11, 13, 16, and 17 adjacent to the broken fiber element decreases as IFSS decreases. This is because interfacial debondings occur along the z-axis on the broken fiber; therefore, stress enhancement is relaxed. The figures also indicate that other intact fibers away from the broken one sustain extra stress in place of adjacent intact fibers.

Figure 7 shows stress distributions of fibers 11 (or 7, 8, 13, 16, 17) and 12 at IFSS = 19.6, 39.2 and 73.5 MPa. At IFSS = 39.2 MPa, two interface elements debonded at both upper and lower sides of the broken fiber element. At IFSS = 19.6 MPa, five interface elements debonded at both sides. We found that, as IFSS decreases, the number of debonding interface elements increases. Therefore, broken fiber 12 cannot recover in stress within a short distance for a small IFSS, as seen in Fig. 7b. In other words, stress recovery function is more reduced by a larger scale of interfacial debondings. Meanwhile, a higher stress is imposed to adjacent intact fibers within a stress recovery length, except for the centered fiber element adjacent to the broken one, as shown in Fig. 7a. Thus, we predict that a lower IFSS tends to generate fiber breaks more easily during loading; therefore it leads to lower composite strength. The next section describes the effect of IFSS on a tensile fracture process of the composite.

3.3. Tensile fracture process

Tensile fracture processes of boron/epoxy composites were simulated using the present FEM simulation model. Figure 8a shows a stress–strain diagram simulated at conditions of $V_f = 0.108$ and IFSS = 39.2 MPa. The stress–strain relation is linear at the initial stage, but changes to a nonlinear behavior from the stress level of arrow A. At this level, one fiber element was broken and two interfacial elements adjacent to the broken one debonded. At the stress level of arrow B, a fiber element different from the one above was broken in isolation; it caused several interfacial debondings similarly to that of level A. At arrows C and D, there were fiber breaks and interfacial debondings at different regions. At arrow E, an intact fiber element was broken, followed by several interfacial debondings. At the same strain level, a fiber element near this broken element was also broken, followed by

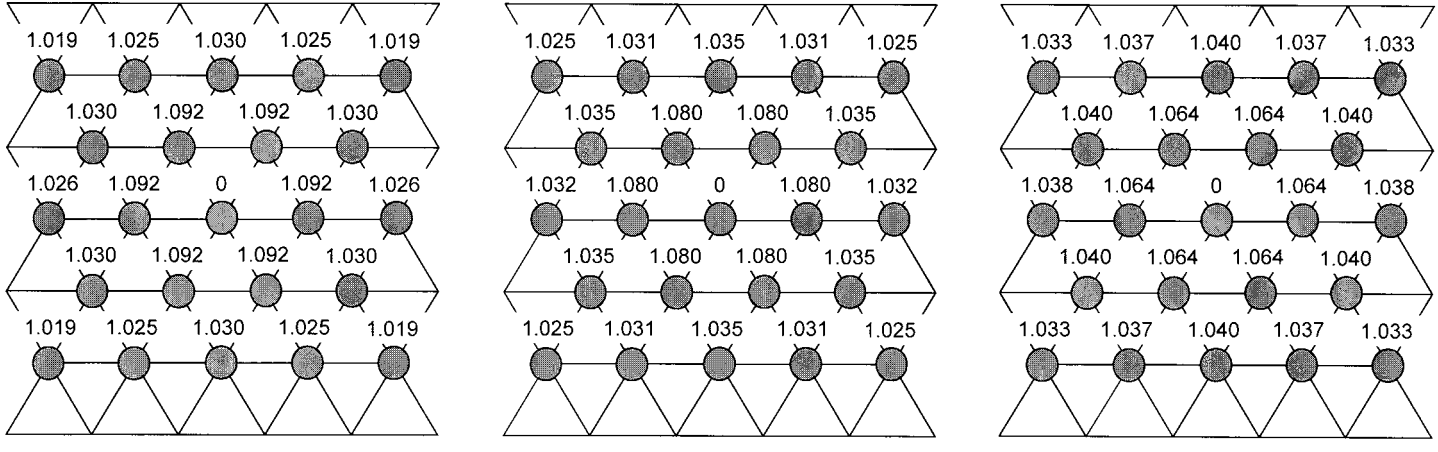

(a) IFSS: 73.5MPa (b) IFSS: 39.2MPa (c) IFSS: 19.6MPa

Figure 6. SCFs to intact fibers in $x-y$ plane located at broken fiber element ($V_f = 0.327$).

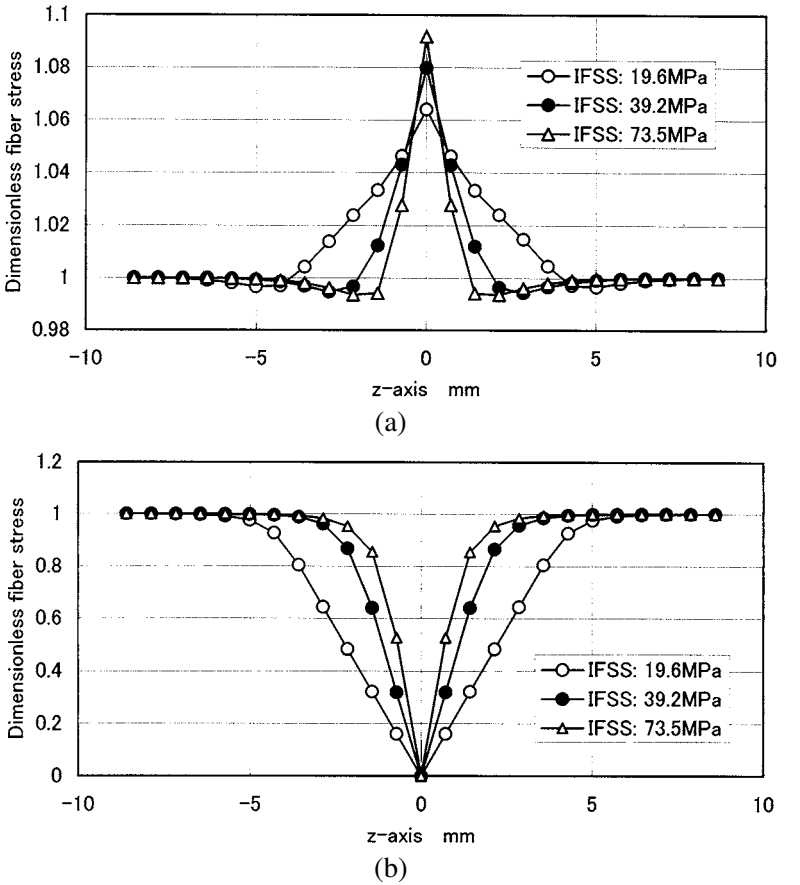

Figure 7. Effect of IFSS on stress distributions of intact and broken fibers ($V_f = 0.327$). (a) Fiber 11. (b) Fiber 12.

several interfacial debondings. At F and G levels, several matrix elements were fractured, following several fiber breaks and interfacial debondings. At arrow H, two fiber elements at the same cross-section were broken, followed by many fiber breaks, interfacial debondings and matrix fractures at the same strain level, and the composite stress decreased. Since the composite stress became less than 80% of the maximum, the calculation was finished. In summary, one fiber element breaks first, followed by interfacial debondings. Next, such damage occurs repeatedly; finally successive fiber breaks, interfacial debondings and matrix fractures occur at the same strain, and cause fracture of the composite. Figures 8b and 8c show simulated stress–strain diagrams for IFSS = 51.5 MPa and 66.2 MPa, respectively. The fiber volume fractions are both 0.108. Simulated fracture processes were similar to that of IFSS = 39.2 MPa in the point that fiber breaks induce interfacial debondings and matrix fractures, but the stress–strain relation becomes more linear for a larger IFSS. This is because the number of debonding interface elements is reduced. It

should be noted in Fig. 8c that many matrix fractures occur at once at the final stage and lead eventually to the composite's fracture. In Fig. 8, tensile strength for IFSS = 51.5 MPa is the highest of all. This implies that an intermediate IFSS

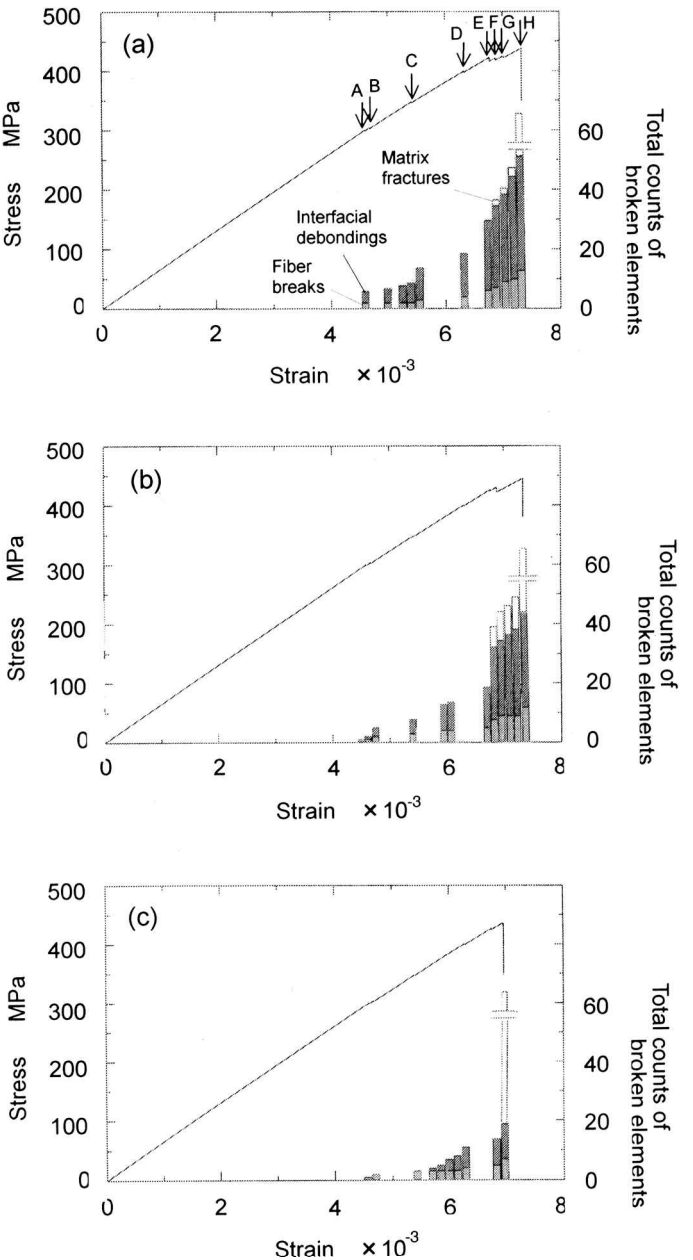

Figure 8. Stress-strain diagrams and total counts of broken elements using the 3D-FEM simulation ($V_f = 0.108$). (a) IFSS = 39.2MPa, (b) IFSS = 51.5MPa, (c) IFSS = 66.2MPa

induces a higher tensile strength. We consider from the above that results obtained here reasonably simulate the tensile fracture process of an actual fiber composite.

3.4. Effect of IFSS on the composite strength

Figures 9a–9c show the effect of IFSS on tensile strength at conditions of $V_f = 0.108, 0.327$, and 0.522, respectively. Results show that as IFSS increases, in all figures, tensile strength first increases, but decreases over the peak. This tendency is quite similar to the result of a two-dimensional fiber array in the previous paper [12]. We consider from such results that there must be an optimum IFSS which raises the tensile strength of unidirectional fiber composites, independent of dimension in a fiber array; IFSSs engendering peak strength are around 50 MPa, 20 to 30 MPa, and 10 to 15 MPa for $V_f = 0.108, 0.327$, and 0.522, respectively. As illustrated in Fig. 7b and Fig. 8a, the number of debonding interface elements increases if IFSS is low. This means that the stress recovery mechanism in broken fibers does not work well; consequently, load carrying capacity in the composite decreases. On the other hand, as seen in Fig. 8c, many matrix fractures ultimately induce a composite fracture. This means that intact fibers are easily broken because of stress enhancement. Thus, we consider that when the number of interfacial debondings is moderate and that of matrix fractures is reduced, higher tensile strengths are

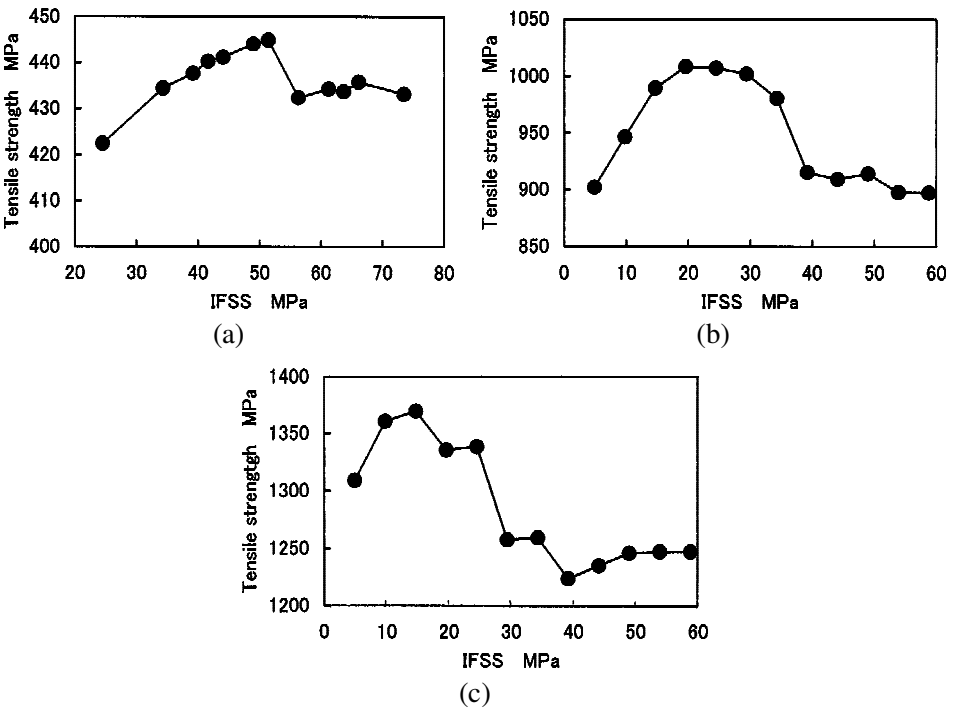

Figure 9. Effect of IFSS on the composite tensile strength using the 3D-FEM simulation. (a) $V_f = 0.108$; (b) $V_f = 0.327$; (c) $V_f = 0.522$.

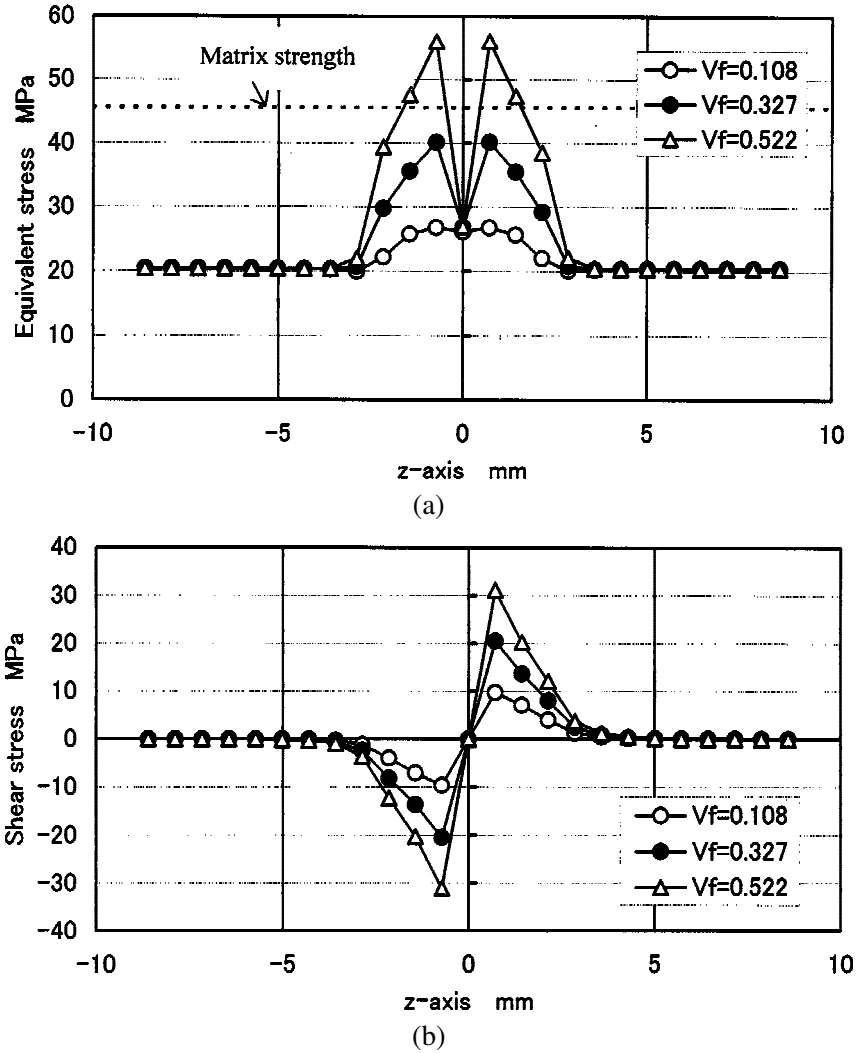

Figure 10. Equivalent and shear stress distributions of the matrices 1 and 6. (a) Equivalent stress of matrix. (b) Shear stress in $y-z$ plane of matrix.

simulated. Such a tendency is obtained in any fiber volume fraction, as shown in Fig. 9, but optimum IFSS is obviously different in each fiber volume fraction. Since the number of fibers included in the composite is identical, this difference must arise from differential fiber spacings. This creates differences among shear stresses in the matrix around fiber breaks.

Figures 10a and 10b show equivalent and shear stress distributions of matrices 1 and 6, respectively, at IFSS $=$ 39.2 MPa, and $V_f = 0.108, 0.327$ and 0.522. The center element of fiber 12 was broken in the same condition as in Section 3.1. It was also assumed that no matrix elements fracture in this case. As shown in Fig. 10a, equivalent stress increases near the center element as fiber volume fraction

increases. Since matrix strength is 45.6 MPa, as shown by the dotted line, matrix elements near the center would be broken in the case of $V_f = 0.522$. Figure 10b shows shear stress distributions of the matrix in the $y-z$ plane. In the cases of $V_f = 0.327$ and 0.522, both interface elements at the upper and lower sides of the center debonded. Despite that, results showed that shear stress increases largely near the center as fiber volume fraction increases. On the other hand, as shown in Fig. 5, normal stress distributions of the matrix at $V_f = 0.108$ and 0.660 were almost in agreement. This means that the magnitude of the matrix normal stress is quite independent of fiber volume fraction. This fact leads us to infer that change in equivalent stress of the matrix arises from that in shear stress. If composite stress further increases, matrix elements would also be broken in the case of $V_f = 0.327$. Such matrix fractures bring stress enhancement to intact fibers and result in decreasing composite stress. This would occur at a lower IFSS, as fiber spacing decreases. Thus, an optimum IFSS, giving the peak of composite strength, decreases if the composite has a higher fiber volume fraction.

4. CONCLUSION

A Monte-Carlo simulation model based on a 3D-finite element method was developed to clarify effects of interfacial shear strength (IFSS) on tensile strength of a unidirectional composite with fibers placed in a hexagonal array. The simulation model was constructed by inserting an interface element between the fiber and matrix elements. As a result of this insertion, the model can simulate interfacial debonding as well as fiber breaks and matrix fractures. Axial tensile fracture processes and strength of a boron-fiber-reinforced epoxy matrix composite were simulated at fiber volume fractions of 0.108, 0.327 and 0.522. Results showed that calculated fiber stress concentration factors on hexagonally-placed intact fibers adjacent to a broken fiber element are comparable to shear-lag solutions of Hedgepeth and van Dyke, and Suemasu. As IFSS decreases, stress concentration factors to intact fibers adjacent to a broken fiber element are reduced because interfacial debonding occurs, while other intact fibers away from the broken one sustain more loads. Interfacial debonding further reduces the load carrying capacity of broken fibers; therefore, composite strength is lowered in any fiber volume fraction. On the other hand, a large IFSS causes many matrix fractures at once and therefore brings a low composite strength. Thus, intermediate IFSSs increased tensile strength of the composite in all fiber volume fractions. This means that there must be an 'optimum' IFSS which induces the highest tensile strength of the composite. The optimum value decreases as fiber volume fraction increases because the matrix around broken fiber elements becomes more apt to be broken easily in shear.

Our future work is intended to further clarify how the effect of IFSS is related to statistical variation in tensile strength of the composite.

REFERENCES

1. J. M. Hedgepeth, Stress concentrations in filamentary structures, NASA Tech. Note, D-882, pp. 1–30 (1961).
2. J. G. Goree and R. S. Gross, Stresses in a three-dimensional unidirectional composite containing broken fibers, *Engng. Fract. Mech.* **13**, 395–405 (1980).
3. S. Ochiai, A. Kengo and K. Osamura, Static stress concentrations due to broken fibers in metal matrix composites with intermediate interfacial bonding strengt, *Z. Metallkde* **76**, 299–306 (1985).
4. H. Fukuda, Stress concentration factors in unidirectional composites with random fiber spacing, *Compos. Sci. Technol.* **22**, 153–163 (1985).
5. K. Goda, S. Tanaka and H. Fukunaga, Stress concentration factors of FRM by shear-lag theory and its statistical treatment, *Trans. JSME* **55A**, 608–613 (1989) (in Japanese).
6. K. P. Oh, A Monte-Carlo study of the strength of unidirectional fiber-reinforced composites, *J. Compos. Mater.* **13**, 311–327 (1979).
7. I. Kimpara, T. Ozaki and S. Takada, Simulation on tensile failure process of unidirectional hybrid FRP, *J. Soc. Mater. Sci., Japan* **34**, 280–285 (1985) (in Japanese).
8. (a) K. Goda and H. Fukunaga, Considerations of the reliability of tensile strength at elevated temperature of unidirectional metal matrix composites, *Compos. Sci. Technol.* **35**, 181–193 (1989); (b) K. Goda and S. L. Phoenix, Reliability approach to the tensile strength of unidirectional CFRP composites by Monte-Carlo simulation in a shear-lag model, *Compos. Sci. Technol.* **50**, 457–468 (1994).
9. S. Ochiai and K. Osamura, Influences of matrix ductility, interfacial bonding strength, and fiber volume fraction on tensile strength of unidirectional metal matrix composite, *Metall. Trans. A* **21A**, 971–977 (1990).
10. T. Okabe, N. Takeda, Y. Kamoshida, M. Shimizu and W. A. Curtin, A 3-D shear-lag model considering micro-damage and statistical strength prediction of unidirectional fiber-reinforced composites, *Compos. Sci. Technol.* **61**, 1773–1787 (2001).
11. K. Goda, Creep-rupture lifetime prediction of unidirectional metal matrix composites with and without time-dependent fiber breakage, *Int. J. Plasticity* **18**, 1729–1748 (2002).
12. (a) K. Goda, Role of interfacial shear debonding in increasing the strength and reliability of fibrer-reinforced composites (Study based on a Monte-Carlo simulation), *Trans. JSME* **63**, 445–452 (1997) (in Japanese); (b) K. Goda, Role of interfacial debonding in increasing the strength and reliability of unidirectional fibrous composites, *Compos. Sci. Technol.* **59**, 1871–1879 (1999).
13. S. L. Phoenix and I. J. Beyerlein, in: *Comprehensive Composite Materials,* Vol. 1, Chapter 1.19. Elsevier Science, Amsterdam, The Netherlands (2000).
14. D. Hull, *An Introduction to Composite Materials.* Cambridge University Press, Cambridge, UK (1981).
15. Z. Maekawa, H. Hamada, A. Yokoyama, K. Lee and S. Ishibashi, Tensile property and its variability on-axis of unidirectional carbon fiber reinforced composites, *J. Japan. Soc. Compos. Mater.* **17**, 155–164 (1991).
16. A. Gatti, J. V. Mullin and J. M. Berry, The role of bond strength in the fracture of advanced filament reinforced composites, *ASTM STP* **460**, 573–582 (1969).
17. J. V. Mullin, Influence of fiber property variation on composite failure mechanisms, *ASTM STP* **521**, 349–366 (1973).
18. S. Takada, I. Kimpara and I. Ohsawa, A finite element analysis model of interlaminar delamination of laminated composites, in: *Proc. Japan–US CCM-V*, Tokyo, pp. 219–226 (1990).

19. C. Bjerken and C. Persson, A numerical method for calculating stress intensity factors for interface cracks in bimaterials, *Engng. Fract. Mech.* **68**, 235–246 (2001).
20. J. M. Hedgepeth and P. Van Dyke, Local stress concentrations in imperfect filamentary composite materials, *J. Compos. Mater.* **1**, 294–309 (1967).
21. H. Suemasu, An analytical study of probabilistic aspects of strength of unidirectional fiber reinforced composites under tensile loads, *Trans. JSCM* **8**, 29–36 (1982).